

PREDICTION OF VERY HIGH REYNOLDS NUMBER COMPRESSIBLE SKIN FRICTION

John R. Carlson*
 NASA Langley Research Center,
 Hampton, Virginia 23681

ABSTRACT

Flat plate skin friction calculations over a range of Mach numbers from 0.4 to 3.5 at Reynolds numbers from 16 million to 492 million using a Navier Stokes method with advanced turbulence modeling are compared with incompressible skin friction coefficient correlations. The semi-empirical correlation theories of van Driest; Cope; Winkler and Cha; and Sommer and Short T' are used to transform the predicted skin friction coefficients of solutions using two algebraic Reynolds stress turbulence models in the Navier-Stokes method PAB3D. In general, the predicted skin friction coefficients scaled well with each reference temperature theory though, overall the theory by Sommer and Short appeared to best collapse the predicted coefficients. At the lower Reynolds number 3 to 30 million, both the Girimaji and Shih, Zhu and Lumley turbulence models predicted skin-friction coefficients within 2% of the semi-empirical correlation skin friction coefficients. At the higher Reynolds numbers of 100 to 500 million, the turbulence models by Shih, Zhu and Lumley and Girimaji predicted coefficients that were 6% less and 10% greater, respectively, than the semi-empirical coefficients.

NOMENCLATURE

A = surface area, $\sum A_i$
 A,B = temperature ratio constants for Van Driest equation
 A_i = incremental surface area
 a = speed of sound
 C_F = average skin friction coefficient
 C_F^* = transformed average skin friction coefficient
 $C_{\epsilon 1}$ = constants for K-e equations
 $C_{\epsilon 2}, C_{\mu}$

c_f = local skin friction coefficient, τ_w/q_{∞}
 D = skin friction drag
 F = shape function
 f_{μ} = near-wall damping function for K - ϵ
 H = total enthalpy
 I = freestream turbulence intensity
 K = turbulent kinetic energy
 k = mixing-length constant
 L = length of flat plate, 5-m
 l = mixing length
 M = Mach number
 N = number of grid points
 n = distance normal to wall
 \bar{P} = production term for turbulent kinetic energy
 p = static pressure, Pa
 q = dynamic pressure, Pa
 R_L = Reynolds number, $(\rho u L)/\mu$
 R_x^* = transformed Reynolds number
 R_T = turbulent Reynolds number, $K^2/(v\epsilon)$
 S = strain tensor
 S_c = Sutherland's constant, 110.33 K
 T = temperature
 T' = intermediate reference temperature
 t = time
 U = velocity
 \bar{U} = magnitude of velocity, $\sqrt{\sum u_k^2}$
 u_k = Cartesian velocity components
 u_{τ}^+ = friction velocity, $\sqrt{\tau_w/\rho_w}$
 u^+ = law-of-the-wall coordinate, U/u_{τ}
 W = vorticity tensor
 x = streamwise distance
 x_i^+ = Cartesian displacement components
 y^+ = law-of-the-wall coordinate, $(\nu u_{\tau})/v$
 y_1^+ = law-of-the-wall height of first cell
 z = vertical distance
 α = free parameter for K turbulent tripping profile
 δ = boundary layer thickness
 ϵ = turbulent dissipation
 γ = ratio of specific heats, 1.4
 θ = boundary layer momentum thickness
 κ = von Karman constant
 μ = laminar viscosity

*Senior Scientist, Aero- and Gas-Dynamics Division.

Copyright 1998 by the American Institute of Aeronautics and Astronautics, Inc. No copyright is asserted in the United States under Title 17, U.S. Code, the U.S. Government has a royalty-free license to exercise all rights under the copyright claimed herein for Governmental purposes. All other rights reserved by the copyright owner.

μ_T	=	turbulent viscosity
μ'	=	viscosity evaluated at T'
ν	=	kinematic viscosity, μ/ρ
ρ	=	density
ρ'	=	density evaluated at T' and p_δ
τ	=	shear stress
ω	=	viscosity power law power, Eqn. 24

Subscripts

aw	=	adiabatic wall
cor	=	correlation reference conditions
i	=	incompressible
L	=	laminar
T	=	turbulent
T'	=	based on temperature T'
t	=	freestream total conditions
w	=	conditions at the wall surface
δ	=	conditions at the boundary layer edge
$\infty, 0$	=	freestream conditions

INTRODUCTION

The efficiency of airplane design has improved considerably as computing power and computer programs have advanced and specialized tools, such as inverse design methods and advanced graphic interfaces, have been developed. Despite this, some fundamental aerodynamic flow issues continue to elude both the experimental- and the computational-based researcher. One such issue involves several aspects of skin friction, specifically, the measurement of skin friction experimentally; the determination of skin friction through parametric correlations; and the prediction of skin friction using advanced computational methods. A survey of some of the semi-empirical theories of skin friction can be found in (Refs. 1–5). Most of the semi-empirical theories were fit to data over a limited range of Mach number and Reynolds number and have had varying degrees of success in obtaining accurate correlations. Typically 5 to 10% error is quoted for the empirical determination of skin friction due in part to scatter and accuracy in the experimental data sets, corrections for model effects and test techniques, and to a small degree, simplifications made in deriving the theories.

The theories chosen for these comparisons will be those of Van Driest, Cope, Winkler and Cha, and Sommer and Short.¹ These correlations will be compared with results from a three-dimensional Reynolds-averaged Navier-Stokes (RANS) code PAB3D (Refs. 6–10) using explicit algebraic Reynolds stress turbulence models for calculations on a 5-meter flat plate with zero pressure gradient. The conditions used for these com-

parisons were Mach numbers from 0.4 to 3.5 at unit Reynolds numbers of 1 to 30 million per foot. Skin friction predictions are compared with the semi-empirical theories. Estimations of solution convergence and errors are discussed. Different transformations of Reynolds number and skin friction are used for several comparisons with the skin friction theories.

COMPUTATIONAL PROCEDURE

Governing Equations

The general three-dimensional Navier-Stokes method PAB3D version 13 was used. This code has several computational schemes and different turbulence and viscous stress models.^{9–10} The governing equations are the RANS equations obtained by neglecting all streamwise derivatives of the viscous terms. The resulting equations are written in generalized coordinates and conservative form. Viscous model options include thin-layer assumptions in any direction or any two indices fully coupled with the third uncoupled. Typically, the fully three-dimensional viscous stresses are reduced to a thin-layer assumption, but this assumption may not always be appropriate. Experiments such as the investigation of supersonic flow in a square duct were found to require fully coupled two-directional viscosity to properly resolve the physics of the secondary cross-flows.⁶

The Roe upwind scheme with third-order accuracy is used in evaluating the explicit part of the governing equations, and the van Leer scheme is used to construct the implicit operator. The diffusion terms are centrally differenced, and the inviscid flux terms are upwind differenced. Two finite volume flux-splitting schemes are used to construct the convective flux terms. The code can utilize min-mod, van Albeda, Spekreijse-Venkat, or modified Spekreijse-Venkat limiters. All solutions were developed with the third-order-accurate scheme for the convective terms and second-order scheme for the viscous diffusion terms. The min-mod limiter was utilized in the blocks containing wall-bounded flow, otherwise the van Albeda limiter was used.

The code can utilize a 2-, 3-factor, or diagonalization numerical scheme to solve the flow equations. The 2-factor scheme can be used when the predominant flow direction is oriented along the i -index of the grid. An example would be a jet-plume or nozzle configuration where the $j-k$ index grids generally represent cross-planes of the exhaust flow. Though this scheme typically requires 10–15% less memory than the 3-factor scheme it is less applicable to many general 3-D aerodynamics problems due to inconsistency between the mesh topologies and the flow solution.

These flow simulations were performed using the 3-factor scheme.

Turbulence Simulation

Version 13 of the PAB3D code used in this study has options for several algebraic Reynolds stress (ASM) turbulence simulations. The standard model coefficients of the $K-\epsilon$ equations were used as the basis for all of the linear and nonlinear turbulent simulations as shown in Table 1.

Table 1. Linear $K-\epsilon$ Standard Coefficients

Constant	Value
$C_{\epsilon 1}$	1.44
$C_{\epsilon 2}$	1.92
C_{μ}	0.09

The near wall damping function of Launder and Sharma,¹¹

$$f_{\mu} = \exp[-3.41/(1 + R_T/50)^2]$$

determined the behavior of ϵ as a function of $R_T = K^2/(v\epsilon)$. The boundary conditions for ϵ and K at the wall are

$$\epsilon_w = 2\nu[(\partial/\partial n)\sqrt{K}]^2$$

and

$$K_w = 0$$

The turbulence model equations are uncoupled from the RANS equations and are solved at the same time step as that of the mean flow solution. Relatively high Courant-Friedrichs-Lewy (CFL) numbers can be used (e.g. $1 \leq CFL \leq 10$) and though rather problem dependent, occasionally flow solution transients can force a temporary time step reduction of the solution of the turbulence equations. More often it is a grid-resolution or grid-quality issue rather than strictly a turbulence modeling difficulty that requires lower CFL numbers to be used. The turbulence equations are solved at all grid levels, not just at the finest grid level.

The algebraic Reynolds stress turbulence model by Girimaji¹² with the Speziale, Sarkar and Gatski (SSG) coefficients¹³ and the model by Shih, Zhu and Lumley¹⁴ (SZL) were utilized in this study. The coefficients of the linear $K-\epsilon$ model were used unmodified as there has not yet been a recalibration performed with any of the ASM's in this code. The model developed by Shih, Zhu

and Lumley is based on the turbulent constitutive relations developed by Shih and Lumley.¹⁵ The model by Girimaji is also based on a set of algebraic relations between the turbulent Reynolds stresses and the mean velocity field but uses the pressure/strain relationship by Speziale et al.¹³ The model is similar to that of Gatski and Speziale¹⁶ except for the determination of the variable coefficient C_{μ} . Further discussion of the turbulence model equations and the algebraic Reynolds stress turbulence model implementation can be found in (Ref. 9).

Turbulent Trip Tactics

The tripping of laminar flow to turbulent can be fixed through the imposition of ϵ and K profiles at user-specified points or grid lines. The line or plane of the specified trip area is surveyed for the maximum and minimum velocity and vorticity, and a shape function from 0 to 1 is created. The shape function, F , is defined as

$$F = \frac{f - f_{\min}}{f_{\max} - f_{\min}}$$

where

$$f = U|W|$$

and

$$|W| = 2\sqrt{\sum W_{ij}^2}$$

f is the product of the velocity, U , and vorticity magnitude, $|W|$. The turbulent kinetic energy profile is then generated using

$$K = \alpha \bar{U} F$$

where α is a free parameter that determines the magnitude of ϵ and K profiles as a percent of the local velocity magnitude \bar{U} . The value used for this paper is 0.1% ($\alpha = 0.001$). The ϵ profile is developed from the assumption that production over dissipation of turbulence is 1, that is, $\bar{P}/\epsilon = 1$. This results in the equation

$$\epsilon^2 = 2C_{\mu}K^2\bar{S}_{ij}(\partial u_i/\partial x_j) \quad (1)$$

The result of the tripping is typically observed as a localized spike in the K field. Depending upon the flow conditions, such as local Reynolds number, momentum Reynolds number, or freestream Mach number, turbulence may or may not develop downstream of the trip point. Turbulence quantities such as the production \bar{P} , or the turbulent stresses $\overline{u'u'}$, $\overline{u'v'}$, ... are left as floating point numbers and are not explicitly set to zero or any

other value “upstream” of trip points. The initial levels of these quantities are determined by thresholds of \sqrt{K}/a and μ_T/μ that are parameters in a user input file. Table 2 lists the limits used for these calculations.

Table 2. Numerical Thresholds for Turbulence Parameters

Constant	Value
\sqrt{K}/a	0.0001
μ_T/μ	0.1

Under some circumstances, these thresholds can be manipulated so as to cause a laminar boundary layer to transition without any explicit tripping specified. As an example, given the freestream conditions of $M = 0.4$, $T_t = 551.8R$, and a unit Reynolds number of 1 million, with $\sqrt{K}/a = 0.0004$, the flat plate flow was fully turbulent. If $\sqrt{K}/a = 0.0001$, transition never occurred. As a point of interest, the lower limit of K can be related to the freestream turbulence intensity, I , as

$$I = \frac{\sqrt{2/3} \sqrt{K}}{M_\infty a} \quad (2)$$

So that $\sqrt{K}/a = 0.0001$ would correspond to a fairly low freestream turbulence intensity of $I \approx 0.02\%$. A proposed lower limit of freestream turbulence intensity to significantly influence transition is 0.08% .¹⁷

Unfortunately the use of the particular ratios, \sqrt{K}/a and μ_T/μ , for setting the lower threshold values for the various turbulent quantities makes a definitive correlation with I difficult because of the relationship between ε at its lower threshold and \sqrt{K}/a . That is,

$$\varepsilon|_{\text{threshold}} = \frac{C_\mu a^2 (\sqrt{K}/a)^2}{(\mu_T/\mu)\mu} \quad (3)$$

μ_T/μ would have to be varied as the square of \sqrt{K}/a to maintain a fixed $\varepsilon|_{\text{threshold}}$ so potentially a correlation between I and transition to turbulence for this configuration could then be developed.

Calculations performed for this paper explicitly set the trip point at the leading edge of the plate. Depending up the freestream Mach number and the unit Reynolds number, transition to turbulence occurred at different locations downstream of the leading edge. A section in Results and Discussion will address this issue further.

SEMI-EMPIRICAL THEORIES

The following is a short review of the theories used in this paper. Discussions of additional theories can be found in (Ref. 1).

Karman-Schoenherr Equation

A number of semi-empirical correlations have been derived for skin friction coefficients with Reynolds number. The basis for most of the correlations in this report is a relationship by Schoenherr derived from the work of von Karman.¹⁸ A numerical fit by von Karman to a set of experimental data resulted in

$$\frac{1}{\sqrt{C_F}} = 4.13 \log_{10}[C_F R_L] \quad (4)$$

C_F and R_L are defined here as

$$C_F = \frac{D/A}{\frac{1}{2}\rho_\infty U_\infty^2} \quad (5)$$

and

$$R_L = \frac{\rho_\infty U_\infty L}{\mu_\infty} \quad (6)$$

though not explicitly defined (Ref. 1), total drag is defined as the summation of the incremental shear stress at the wall times the incremental area,

$$D = \sum_i \tau_{w,i} A_i \quad (7)$$

Equation 4 is a result of a number of simplifications and assumptions about the character of an incompressible boundary layer. Typically, the viscous sublayer below $y^+ \approx 11.5$, is neglected and the velocity gradient at the low end of the log-layer region, $11.5y^+ \leq n \leq 0.2\delta$, is set equal to 0.218 .¹⁹ Additionally, the turbulent stress in the log-layer region is assumed constant and equal to the laminar stress at the wall. This assumption simplifies the solution of the velocity distribution (to be discussed in the following paragraphs) for a specific wall shear-stress which would be associated with a particular skin-friction coefficient and set of free-stream conditions and is fairly consistent with the nature of the total stress in the boundary layer. Figure 1 shows the interplay between the laminar stress and turbulent stress in the boundary layer for $M = 0.4$, $R = 1$ million/ft. near the trailing edge of the flat plate ($R_L = 15.8 \times 10^6$).

The cross-over in the stresses occurs at approximately $y^+ = 10$ which is fairly close to the previously stated assumption of 11.5 . The log-layer extends to approximately 0.2δ which is in this case is $y^+ \approx 1400$, and the turbulent stress in the log-layer is observed to be slightly less than that of the laminar stress at the wall. The boundary layer velocity profile is plotted for visual reference.

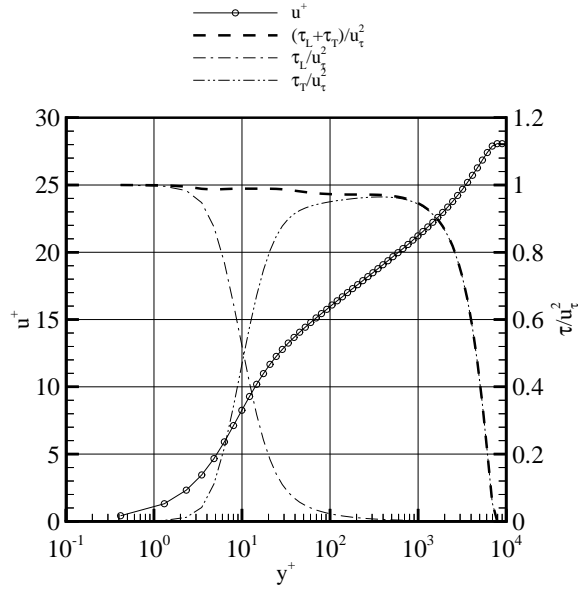


Figure 1. Laminar and turbulent stresses in boundary layer.

Historically, either Prandtl's ($l = \kappa n$) or von Karman's ($l = \kappa(du/dn)/(d^2u/dn^2)$), theory have been used for the mixing-length l and will produce similar forms for the skin friction equation (Eqn. 4) but different coefficients on either side of the relation. Subsequent to this, various techniques have been applied to deriving the skin-friction relationships. The von Karman momentum integral (Eqn. 8) is the basis for relating the skin friction and Reynolds number. Since the integral equation is quite intractable analytically, several alternate representations (typically numerical approximations) of the integral have been derived.¹⁹

$$\tau = \frac{d\theta}{dx} = \frac{d}{dx} \int_0^{\delta} \frac{\rho u}{\rho_{\infty} u_{\infty}} \left(1 - \frac{u}{u_{\infty}}\right) dz \quad (8)$$

Van Driest Method

Van Driest's analysis used Prandtl's mixing length and an interpolation expression representing von Karman's integral equation considering for the effects of compressibility. This resulted in the following equation from (Ref.1).

$$\frac{0.242}{\sqrt{C_{F,w}}} \phi = \log_{10} \left[C_{F,w} R_{L,w} \left(\frac{T_{\delta}}{T_w} \right)^{1/2} \right] \quad (9)$$

where

$$\phi = \frac{1}{A} \left[\text{asin} \frac{\bar{A} - \bar{B}}{2\bar{A}} + \text{asin} \frac{\bar{B}}{2\bar{A}} \right] \quad (10)$$

$$\bar{A}^2 = \frac{T_{aw}}{T_w} - \frac{T_{\delta}}{T_w} \quad (11)$$

and

$$\bar{B} = \frac{T_{aw}}{T_w} - 1 \quad (12)$$

$C_{F,w}$ and $R_{L,w}$ are defined as:

$$C_{F,w} = \frac{D/A}{\frac{1}{2} \rho_w U_{\delta}^2} \quad (13)$$

and

$$R_{L,w} = \frac{\rho_w U_{\delta} x}{\mu_w} \quad (14)$$

An alternate form of the factors A and B are published in (Ref. 19) using Mach number and temperature. Equations (11) and (12) are equivalent to the following equations, Eqs. (15) and (16), if the boundary layer edge conditions, δ , are taken to be the same at the free-stream conditions and $T_{aw} = T_t$.

$$\bar{A}^2 = \frac{\frac{\gamma-1}{2} M_{\infty}^2}{T_w/T_{\infty}} \quad (15)$$

and

$$\bar{B} = \frac{1 + \frac{\gamma-1}{2} M_{\infty}^2}{T_w/T_{\infty}} - 1 \quad (16)$$

Both Van Driest and the theory by Cope evaluate quantities by the conditions at the wall and an outside reference. Reference 1 is not explicit in the outside reference condition definition. The subscript δ was defined as "conditions outside the boundary layer," whether that implies free-stream conditions or the conditions at the point of $U/U_{\infty} = 0.995$, which by definition place some flow quantities 0.5% less than free-stream, is not discernible. For the flat plate cases considered in this report, the reference shift results in slight shifts in both

Reynolds number and skin friction, such that the resultant numbers remain generally along the same curve.

Cope Method

The theory by Cope, rather than working from a mixing length law, assumes that the compressible velocity profile can be transformed to the incompressible profile by using the wall density and viscosity. The resulting equation is shown.

$$\frac{0.242}{\sqrt{C_{F,w}}} = \log_{10} \left[C_{F,w} R_{L,w} \frac{T_\delta}{T_w} \right] \quad (17)$$

Winkler and Cha Method

The theory by Winkler and Cha uses a different scaling assumption for arriving at the compressible skin friction, i.e.,

$$c_f/c_{f,i} \Big|_{R_\theta = \text{Constant}} = \frac{(T_w/T_{aw})^{1/4}}{(T_t/T_\infty)^{1/2}} \quad (18)$$

and results in the following equation

$$\frac{0.242}{\sqrt{C_F (T_t/T_\infty)^{1/2} (T_w/T_{aw})^{-1/4}}} = \log_{10} [C_F R_L] \quad (19)$$

where now C_F and R_L are defined as previously discussed under the Karman-Schoenherr equation section. For this correlation all quantities are evaluated at free-stream conditions, with the exception of the total drag integration which the author assumes still utilizes the viscosity at the wall for the determination of the wall shear stress.

Sommer and Short T' method

The T' method utilizes an empirical relationship between the Mach number and temperature at the edge of the boundary layer, and the wall temperature to arrive at a reference temperature at which the properties (density and viscosity) of the boundary layer are evaluated. Several equations have been proposed, as discussed in (Ref. 1), but only the method of Sommer and Short will be shown.⁵ The reference temperature is calculated from

$$\frac{T'}{T_\delta} = 1 + 0.035 M_\delta^2 + 0.45 \left(\frac{T_w}{T_\delta} - 1 \right) \quad (20)$$

The skin friction formula then has the form

$$\frac{0.242}{\sqrt{C_{F,T'}}} = \log_{10} [C_{F,T'} R_{L,T'}] \quad (21)$$

where $C_{F,T'}$ and $R_{L,T'}$ are now evaluated at the reference

conditions as follows:

$$C_{F,T'} = \frac{D/A}{\frac{1}{2} \rho' U_\delta^2} \quad (22)$$

and

$$R_{L,T'} = \frac{\rho' U_\delta x}{\mu'} \quad (23)$$

Each theory has a different set of normalizations and are shown in Table 3.

Table 3. Summary of Theories

Theory	C_F^*	R_L^*
Van Driest	$\frac{C_{F,w}}{\phi^2}$	$\frac{R_{L,w} \phi^2}{(T_w/T_\delta)^{1/2}}$
Cope	$C_{F,w}$	$\frac{R_{L,w}}{T_w/T_\delta}$
Winkler and Cha	$C_F \frac{(T_t/T_\delta)^{1/2}}{(T_w/T_{aw})^{1/4}}$	$R_L \frac{(T_w/T_{aw})^{1/4}}{(T_t/T_\delta)^{1/2}}$
Sommer and Short T'	$C_{F,T'}$	$R_{L,T'}$

The skin friction coefficient calculated by the Navier-Stokes (NS) method, are non-dimensionalised by different coefficients than most of the correlations. The definitions for skin friction, C_F and Reynolds number, R_L in the computational method are the same as Eqs. (5) and (6); therefore, the transformations shown in Table 4 are required to compare the computational results with most of the correlations.

Table 4. Summary of computational transformations

Correlation Reference	$C_{F,cor}$	$R_{L,cor}$
Wall	$C_F \frac{T_w}{T_\delta}$	$R_L \frac{(T_w/T_\delta)^{-1}}{\mu_w/\mu_\delta}$
T'	$C_F \frac{T'}{T_\delta}$	$R_L \frac{(T'/T_\delta)^{-1}}{\mu'/\mu_\delta}$
Free Stream	C_F	R_L

For simplicity in the analysis, several theories use the single power relation of

$$\mu_w/\mu_\delta = (T_w/T_\delta)^\omega \quad (24)$$

where typically $\omega = 0.76$. A slightly more accurate relation is Sutherland's law.

$$\frac{\mu_w}{\mu_\delta} = \left(\frac{T_w}{T_\delta}\right)^{1.5} \left(\frac{T_\delta + S_c}{T_w + S_c}\right) \quad (25)$$

Figure 2 shows the difference in the viscous ratio using the power law compared to Sutherland's law. The temperature T is substituted for T_w when those reference conditions are used. For temperature ratios less than 2, the viscosity scaling error would be 5% or less using the power law compared to Sutherland's law. Since temperature ratio ranged from 1.02 at $M = 0.4$ to 2.41 at $M = 3.5$, the Sutherland's law relation was utilized for post processing the skin friction predictions.

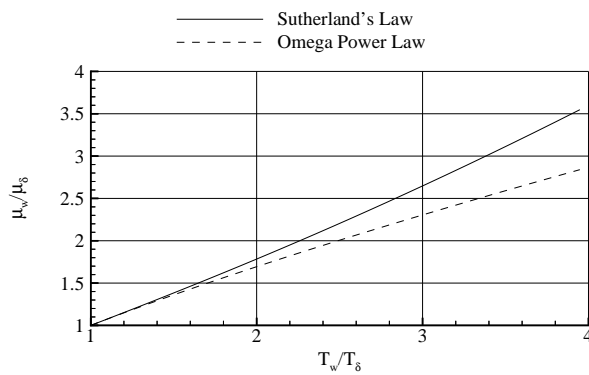


Figure 2. Viscosity ratio from temperature ratio.

Solution Process

Turbulent flow solutions that use ASM and the two-equation linear $K - \epsilon$ model require 23 words of memory per grid point. The code speed is dependent on the turbulence model, viscous model assumptions, and numerical schemes. All solutions for this study were performed on Silicon Graphics workstations. The code was compiled using Fortran 90, double-precision (64-bit) with O2 level of optimization. The code speed at the finest grid level was approximately 110 microseconds/iteration/grid point running a 3-factor solution scheme, 1 thin-layer viscous direction and using an algebraic Reynolds stress turbulence model. The computer memory requirement was approximately 18 megabytes.

Solution residual and total skin friction were used to gauge solution convergence. Total skin friction was solution converged and grid converged.

RESULTS AND DISCUSSION

Determination of Boundary Layer Edge Criteria

An accurate and consistent determination of the edge of the boundary layer is important for calculation of momentum thickness Reynolds number, shape factors, and edge conditions. The skin friction correlation, R_θ vs c_f , was used to evaluate the applicability of several velocity and enthalpy edge values. Figures 3 through 5 are the two criteria for $M = 0.4$ and figures 6 through 8 are for $M = 1.2$ at the Reynolds number of 1 million/ft. The skin friction and Reynolds numbers plotted here are evaluated using free stream values. At $M = 0.4$, the laminar and turbulent coefficients are consistent up to the velocity edge criteria of 0.995. The enthalpy edge criteria is consistent up to 0.99. The equivalence of the two criteria for this condition is shown in figure 5.

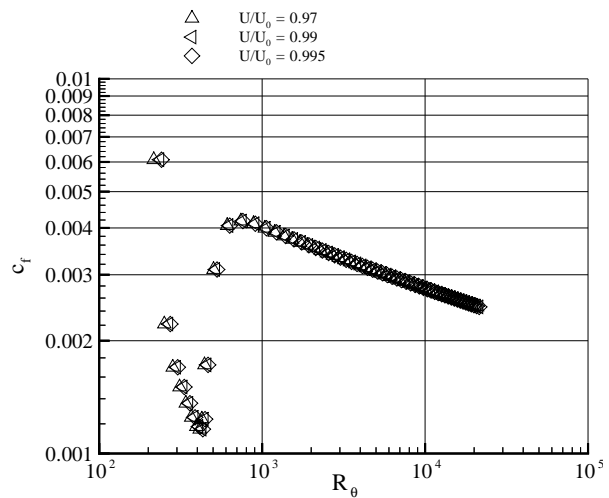


Figure 3. Velocity edge criteria $M = 0.4$, $R = 1$ million/ft.

The transonic case, $M = 1.2$, required much lower edge criteria, (Figs. 6 and 7). With the exception of the first cell, the velocity criteria of 0.98 and enthalpy criteria of 0.97 give fairly consistent results for the skin friction correlation. These two criteria are plotted in figure 8 and show similar results. For the higher supersonic conditions of Mach = 2.4 and 3.5, a consistent boundary layer edge could be determined with the enthalpy criteria as high as 0.995. The choice of which edge criteria is used results in different temperature and viscosity values being used in determination of the boundary layer

edge conditions. Recall that the semi-empirical theories of Cope and Sommer and Short used boundary layer edge conditions for the scaling of the skin friction and Reynolds number rather than the free-stream. No matter which criteria is applied, the edge conditions will be slightly different than the free-stream. The variation of the edge velocity is plotted in figures 9 and 10 for the two edge criteria at $M = 0.4$ and 1.2 . The two edge criteria produce very similar edge velocities for the subsonic case, but the particularly difficult transonic condition of $M = 1.2$, determines significantly different edge velocities depending upon the criteria chosen.

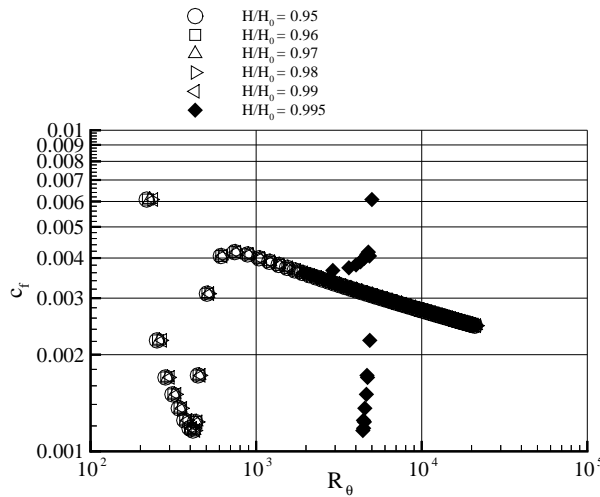


Figure 4. Enthalpy edge criteria $M = 0.4$, $R = 1$ million/ft.

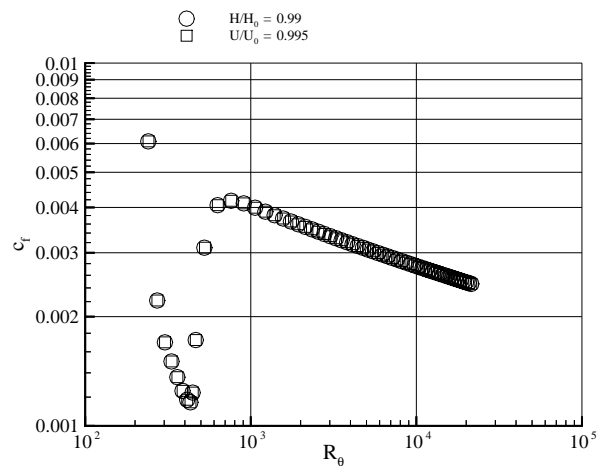


Figure 5. Equivalence of velocity and enthalpy edge, $M = 0.4$, $R = 1$ million/ft.

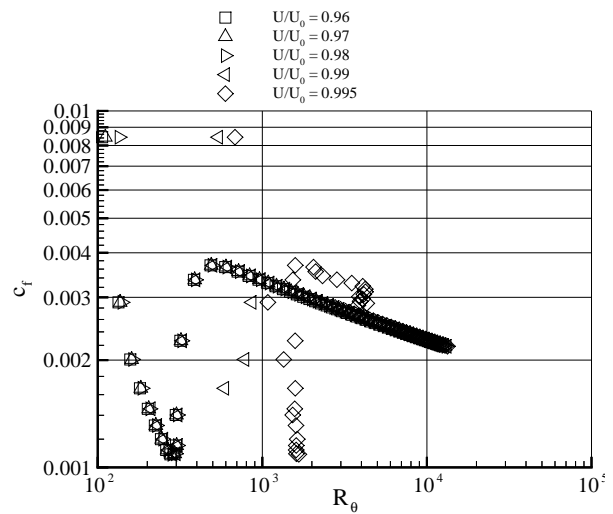


Figure 6. Velocity edge criteria at $M = 1.2$, $R = 1$ million/ft.

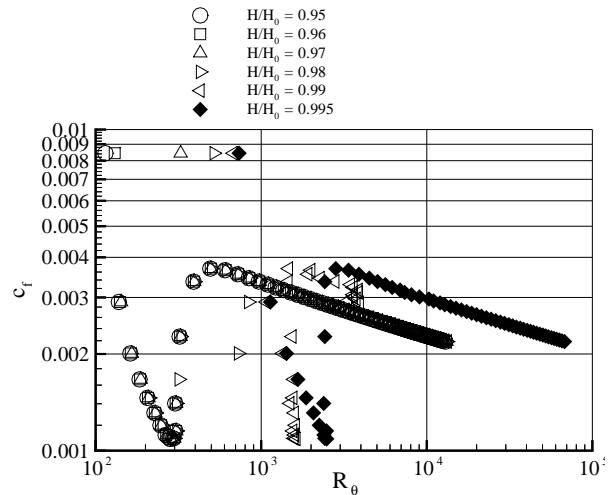


Figure 7. Enthalpy edge criteria at $M = 1.2$, $R = 1$ million/ft.

ESTIMATION OF LAMINAR-TO-TURBULENT FLOW RATIO EFFECTS

Laminar flow present in a computational flow solution changes the predicted skin friction from that of an assumed fully turbulent flow. For a given physical geometry, obviously the Reynolds number of the problem is a major factor in determining the degree of laminar flow that might exist. Secondly, the existence of laminar flow in the CFD solution is also dependent

upon whether there is sufficient grid density to actually predict the laminar flow. Assuming an incompressible flow with a critical Reynolds number of 500,000, Table 5 is an estimation of the expected laminar run for the 5-m flat plate at different unit Reynolds numbers. The third column is an estimation of the percentage of the flow that would be laminar. The fifth and sixth columns are the two terms of an expression for total skin friction derived in Schlichting¹⁸ accounting for the initial laminar region. The first term is the regular expression for fully turbulent flat plate skin friction and the second term is a correction for the laminar segment.

$$C_F = \frac{0.074}{\sqrt{R_L}} - \frac{A}{R_L}, \quad 5 \times 10^5 < R_L < 10^7$$

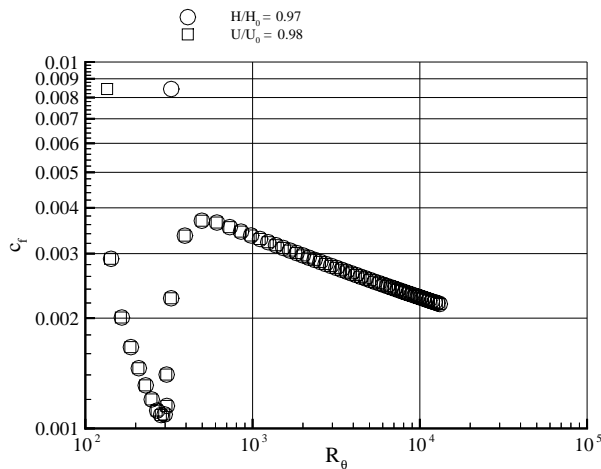


Figure 8. Equivalence of velocity and enthalpy edge, $M = 1.2$, $R = 1$ million/ft.

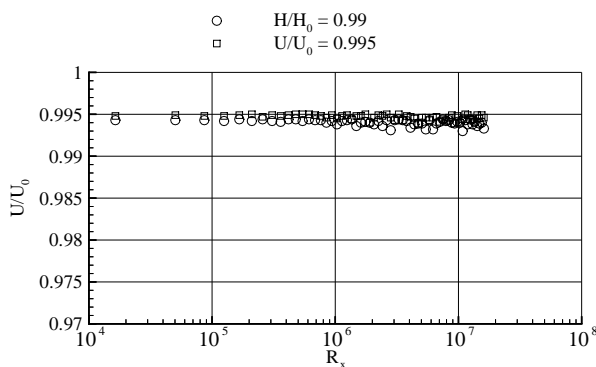


Figure 9. Normalized velocity at boundary layer edge, $M = 0.4$, $R = 1$ million/ft.

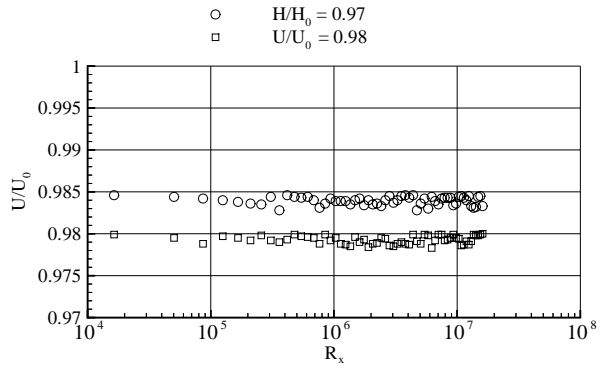


Figure 10. Normalized velocity at boundary layer edge, $M = 1.2$, $R = 1$ million/ft.

Figure 11 shows the variable A as a function of critical Reynolds number. The quoted Reynolds number range of applicability is less than 10^7 , so it must be noted that applying it to the present problem is an extrapolation of this equation. At Reynolds numbers greater than 4 million per ft., the laminar aspect of the flat plate flow becomes less than 1/2 of 1 percent of the total length of the plate. Additionally, the estimated decrease in total skin friction coefficient is less than 0.00003. Therefore, a leading edge spacing of 0.01 m should be sufficient to predict the laminar flow at the lower Reynolds numbers. It is inadequate to resolve any laminar flow in the high Reynolds number range, but the degree of error in total skin friction coefficient is estimated to be less than 0.00003.

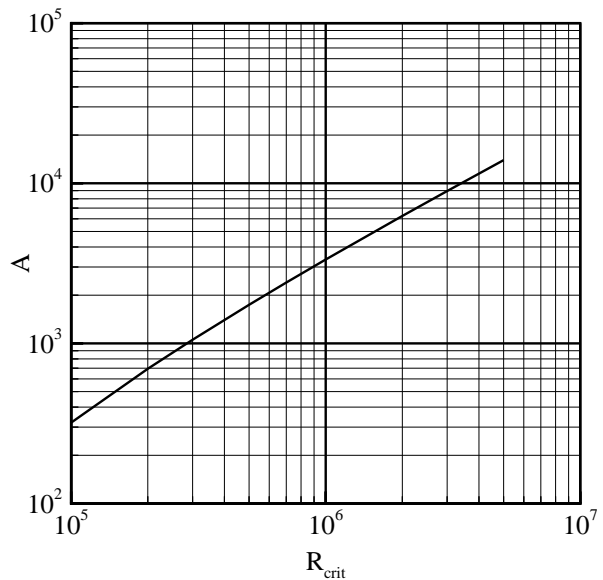


Figure 11. Variation of constant A with critical Reynolds number.

Table 5. Estimation of laminar flow contribution to total skin friction coefficient

Reynolds number (million/ft.)	Reynolds number (million)	Est. Laminar run, x (m)	x/L (%) L=5 m	$\frac{0.074}{\sqrt[5]{R_L}}$	$-A/R_L$
1.	16.	0.1524	3.0	0.00268	-0.00010
2.	32.	0.0762	1.5	0.00233	-0.00005
4.	65.	0.0381	0.8	0.00203	-0.00003
8.	131.	0.0191	0.4	0.00176	-0.00001
15.	246.	0.0102	0.2	0.00155	-0.00001
30.	492.	0.0051	0.1	0.00135	-0.00000

Flat-Plate Grid

The 5-m flat-plate multiblock grid had an H-type mesh topology, with three blocks placed streamwise. The computational domain included an inflow block, block 1, extending 2.5 m upstream from the leading edge of the 5-m flat plate. The plate, block 2, had an initial streamwise grid spacing at the leading edge of 0.01 m and was exponentially stretched from the leading edge to the trailing edge at a rate of 6.7% using a total of 61 grid points. Block 3, downstream of block 2, was 2.5 m long. This was to displace the outflow boundary away from the plate trailing edge. The first cell height of the baseline grid was varied according to the unit Reynolds number as shown in Table 6. The first cell height was fixed at both ends of the plate and exponentially stretched from the surface to the outer boundary. The upper boundary was 20 m away and the lateral width of the grid was 0.098 m.

The grids had the following dimensions.

Table 6. Reynolds number variation of grid spacing at surface

Reynolds number (million/ft.)	y_1 (10^{-6} m)	y_1^\dagger	Initial grid stretching rate
1.	7.50	0.42	14%
2.	3.20	0.34	15%
4.	1.80	0.37	16%
8.	0.94	0.37	17%
15.	0.50	0.35	18%
30.	0.25	0.34	19%

Table 7. Grid dimensions

Block	i-dim	j-dim	k-dim
1	11	2	121
2	61	2	121
3	13	2	121

Grid Convergence

One subsonic case and one supersonic case are shown as representative grid convergence trends. Figures 12 and 13 show total skin friction predictions with inverse of total grid count for $M = 0.4$ and 1.2 respectively, at several different unit Reynolds numbers. Each computation was run out to establish solution convergence at each grid level so that total drag varied less than 0.00005 for several hundred iterations. Additionally, the difference in total skin friction coefficient between the medium and fine density meshes was within 0.00005 for all unit Reynolds numbers except 1 million/ft. where the two levels were within 0.00008 at $M = 0.4$. Slightly better grid convergence was obtained at $M = 1.2$. These variations within the same bounds of error are documented for the incompressible calculations.⁹

Transition to Turbulent Flow

As mentioned earlier, explicit tripping was placed at the leading edge of the flat plate. Transition to turbulent flow occurred at different locations downstream depending upon the freestream conditions. The point at which the flow actually transitioned was determined for each solution by first calculating the peak of the ratio of turbulent viscosity to the local bulk viscosity

at each point along the plate. In regions of laminar flow, this ratio was nominally a constant between 1 to 10 depending upon conditions. Then, at the onset of the development of turbulence, the ratio increases rapidly, typically changing by several orders of magnitude. Figure 14 is a plot of the turbulent viscosity ratio against distance downstream of the leading edge. This trend is representative of solutions with some region of laminar flow upstream of the transition point. In this case, transition occurred at approximately $x = 0.02$ m, which is equivalent to a local Reynolds number of 0.58 million. The symbols are an indication of the streamwise distribution of the grid along the plate.

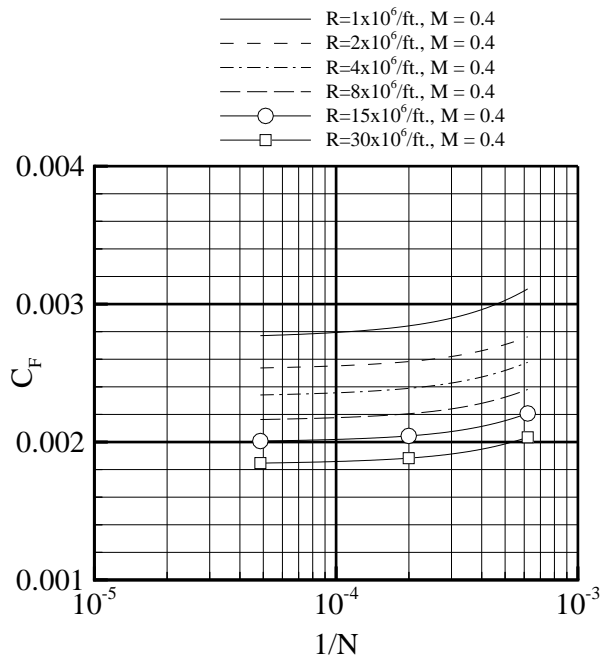


Figure 12. Grid convergence of total skin friction for $M = 0.4$.

Figure 15 is the compilation of the location of transition with Mach number for each unit Reynolds number. The open symbols are solutions in which there were less than 7 cells of laminar flow and the filled symbols are the transition points for solution with greater than 7 cells. Critical Reynolds number is typically quoted as extending from 0.3 to 3 million¹⁸. The flat plate flow transitioned close to, but not always within, these values when greater than 6 cells were upstream of the transition point for unit Reynolds numbers less than 8 million/ft. As discussed in the first section, at unit Reynolds number of 8 million/ft. or greater, there is little expectation

of realizing a laminar flow solution. There is some variation of critical Reynolds number with Mach number at unit Reynolds number greater than 8 million/ft., but this is due to the change in local Reynolds number of the first cell and not due to any physical shift in the transition point. Even if there were sufficient grid density in the leading edge region to capture the laminar flow aspect of the higher Reynolds number flows, the error in skin friction is estimated to be limited to 0.00001.

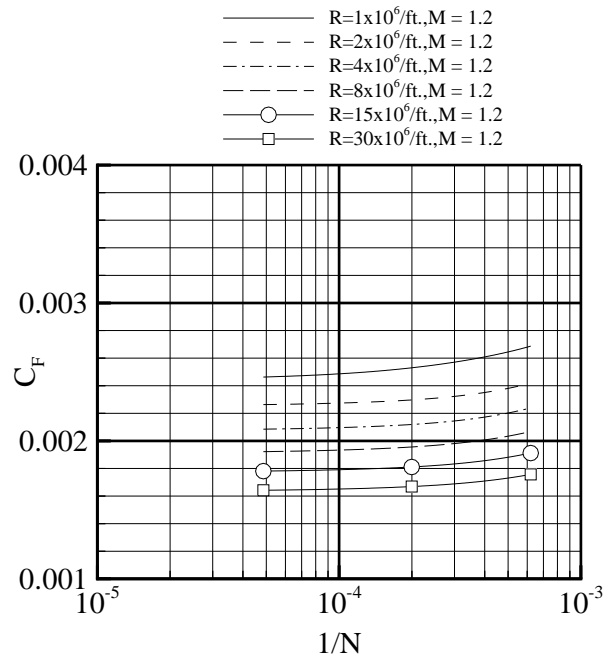


Figure 13. Grid convergence of total skin friction for $M = 1.2$.

Total Skin Friction

The T' theory of Sommer and Short using the Karman-Schoenherr skin friction equation is plotted in figure 16 for the two Mach numbers of 0.10 and 3.50. As per the theory's design, the fully turbulent lines collapse to the same skin friction values, as do the partially laminar estimations. The difference between the incompressible and compressible lines are the transformed Reynolds numbers R^* that occur at each Mach number that can be seen by the offset in the open and closed symbols. The Mach 3.50 results would predict skin friction coefficients significantly less than the incompressible results if plotted using untransformed skin friction and Reynolds number due to changes in both dynamic pressure and kinematic viscosity.

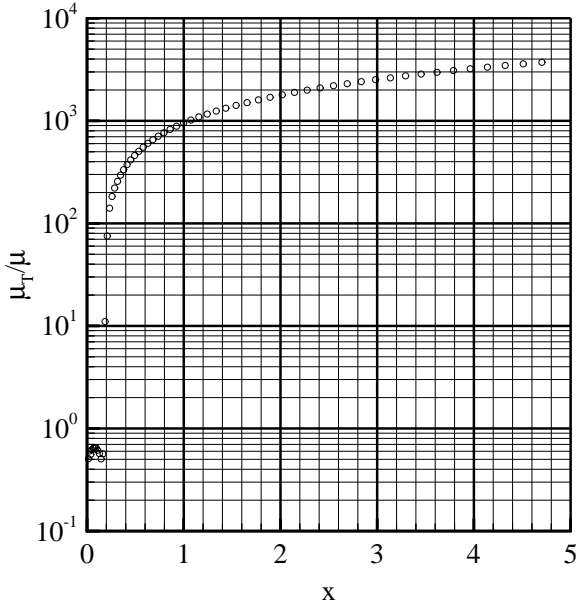


Figure 14. Viscosity ratio growth with distance, $M = 1.2$, $R_L = 1$ million/ft.

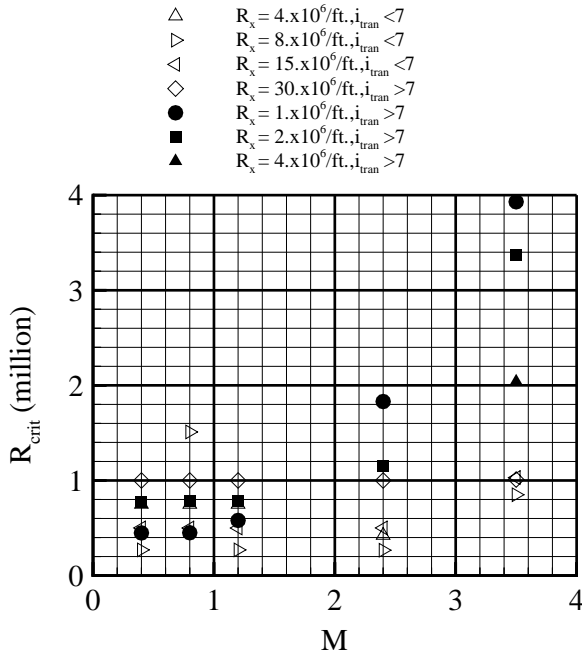


Figure 15. Critical Reynolds number with Mach number, Girimaji ASM.

The computations are compared with the four skin friction theories in figures 17 through 20. The solid line and dashed lines are each theory's fully turbulent

and partially laminar (assuming a critical Reynolds number of 500,000) total skin friction coefficients. The apparent shifting of the same computational result plot-to-plot are the result of the specific transformation required to make the comparisons for each semi-empirical method.

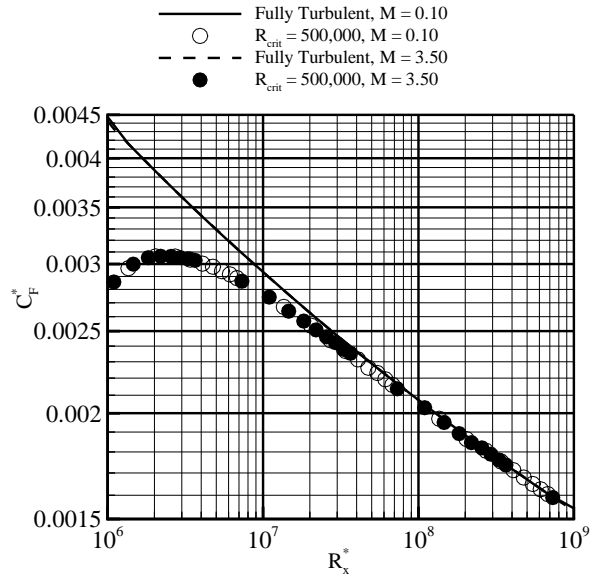


Figure 16. Sommer and Short T' theory at low and high Mach numbers.

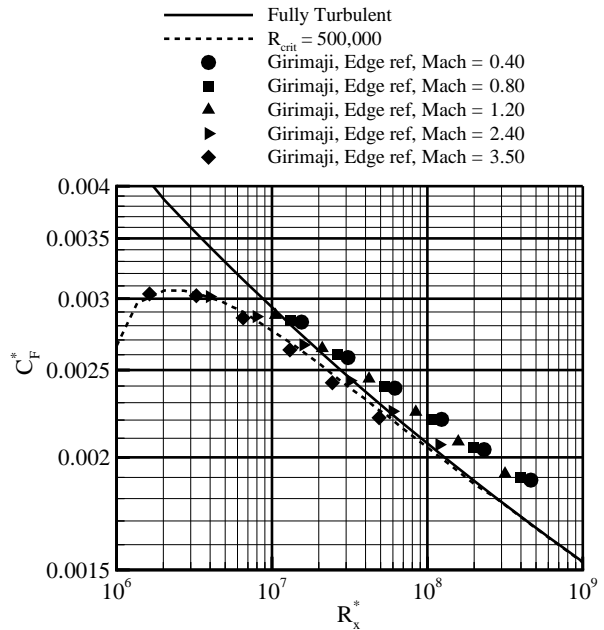


Figure 17. CFD transformed by Van Driest theory compared with incompressible skin friction coefficients.

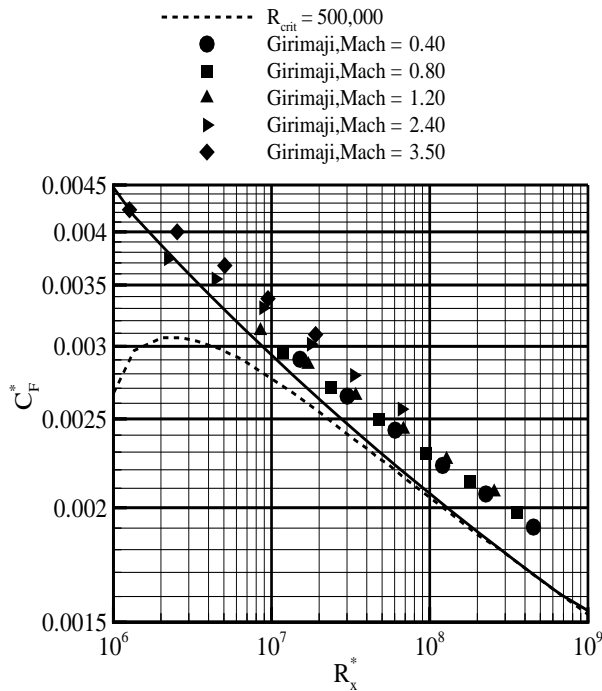


Figure 18. CFD transformed by Cope theory compared with incompressible skin friction coefficients.

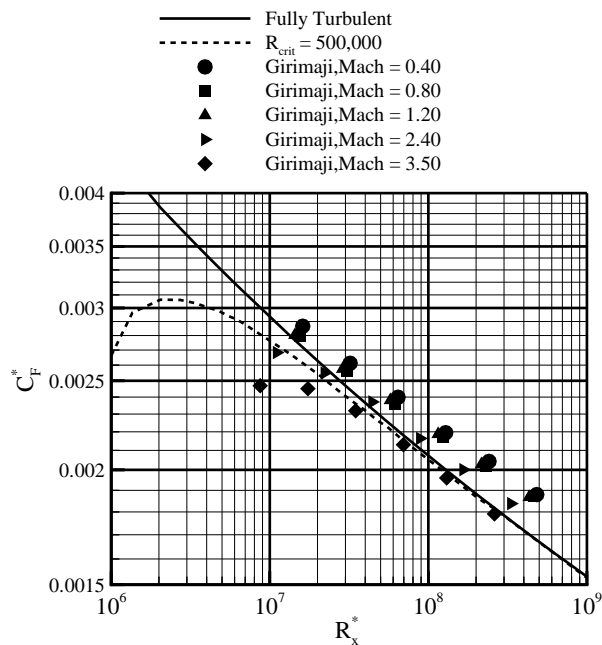


Figure 19. CFD transformed by Winkler and Cha theory compared with incompressible skin friction coefficients.

The skin friction coefficients predicted by the Girimaji turbulence model consistently transformed approximately 0.0002 greater than the incompressible skin friction curve for Reynolds numbers greater than

100 million regardless of the semi-empirical theory used. The high Mach number, low Reynolds number cases which had the larger extent of laminar flow matched very closely the incompressible skin friction curve using either the van Driest or Sommer and Short theories to transform the CFD. Interestingly, the use of wall quantities with Cope did not bring the skin frictions down to the partially laminar theory curve. The transformations with Winkler and Cha did not transform the Reynolds number with increasing Mach number as much as van Driest or Cope, though the fall off in skin friction coefficient for $M = 3.5$, $R = 1$ million/ft. is at least discernible.

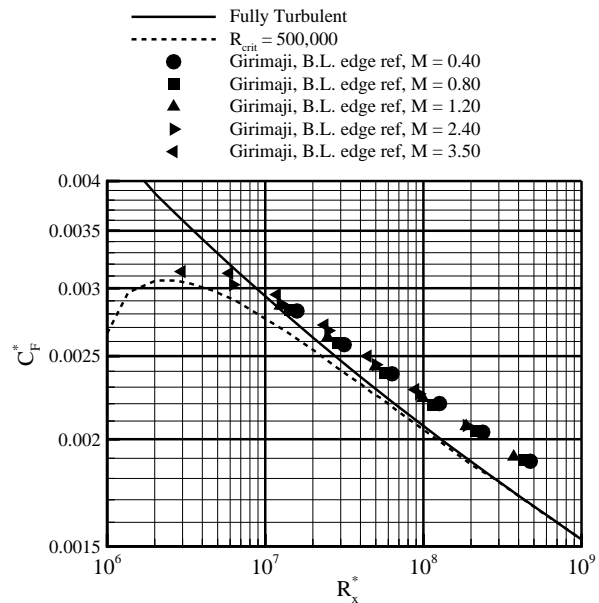


Figure 20. CFD transformed by Sommer and Short T' with Karman-Schoenherr theory compared with incompressible skin friction coefficients, edge reference conditions, Girimaji model.

The theory by Sommer and Short explicitly calls out use of the conditions at the edge of the boundary layer in the equation of determination of the reference temperature. As a result of the fairly benign nature of the flat plate flow, the use of free-stream values for Mach number and temperature appear not to significantly alter the comparison of the incompressible curves and the transformed CFD, as seen in figure 21, as compared to figure 20. In addition, use of either set of reference values did not affect how well the predicted skin friction coefficients collapsed to a single curve. Figure 22 is a comparison of skin friction with flat plate Reynolds number with CFD using the ASM by Shih, Zhu and Lumley. These calculations collapse to the incompressible data similar to the results using the

Girimaji model, except for a slight shift below the correlations. These results are very similar to the incompressible calculations of Ref. 9.

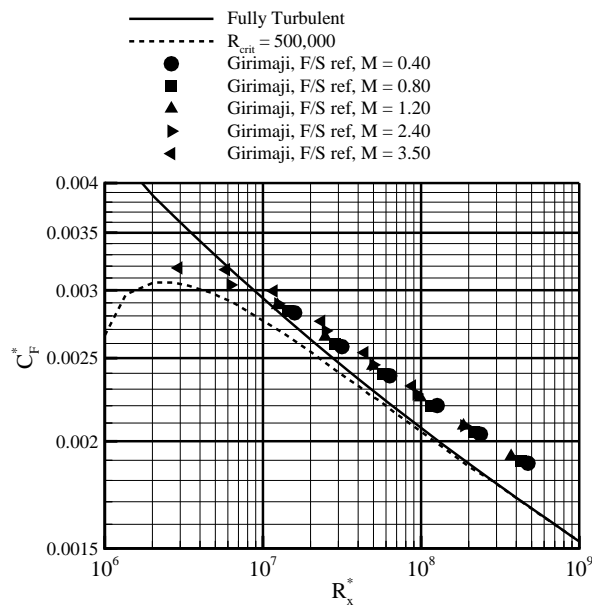


Figure 21. CFD transformed by Sommer and Short T' with Karman-Schoenherr theory compared with incompressible skin friction coefficients, free-stream reference conditions, Girimaji model.

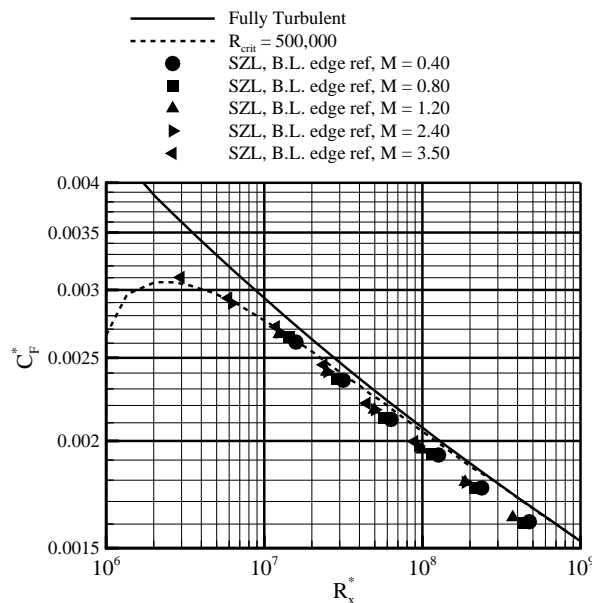


Figure 22. CFD transformed by Sommer and Short T' with Karman-Schoenherr theory compared with incompressible skin friction coefficients, boundary layer edge reference conditions, Shih, Zhu and Lumley model.

If the total stress in the boundary layer is examined, a potential reason for the difference in predicted skin friction between the two turbulence models (Girimaji and Shih, Zhu and Lumley) can be seen. Figures 23 through 25 present the total shear stress predicted by the two turbulence models. Figures 23 and 24 present calculations at $M = 0.4$ at a local Reynolds number of 444 million ($R = 30$ million/ft., near the trailing edge of the plate) which are compared with data from reference 20. Figure 25 presents a calculation at $M = 1.2$ at a local Reynolds number of 14.2 million. The log scale for y/δ in Figures 24 and 25 expands the inner region for clarity, though the lack of data preclude solid conclusions about the comparisons in that region of the boundary layer. A boundary layer profile is plotted on the opposite axis for reference in figure 23. Additionally, Tables 8 and 9 are a sample of the wall values predicted by the two turbulence models at the station plotted for each Mach number. The Girimaji model predicts a higher level of total stress, velocity and friction velocity compared to predictions using Shih, Zhu and Lumley. The Girimaji model also predicts a higher overall total stress level in the boundary layer above $y/\delta = 0.2$, as seen by the dashed line in figure 23. Possibly the prediction of a higher total shear stress in the log-layer region by Girimaji results in over-prediction of the wall skin friction coefficient. At the lower Reynolds number, $R_x = 14.2$ million, where the two models are less different, the total stress in the boundary layer is also more closely matched.

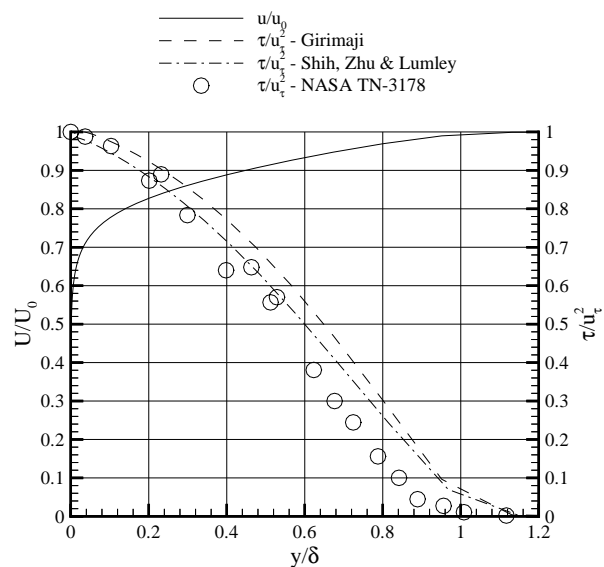


Figure 23. Comparison of total shear stress in the boundary layer, $M = 0.4$, $R = 30$ million/ft.

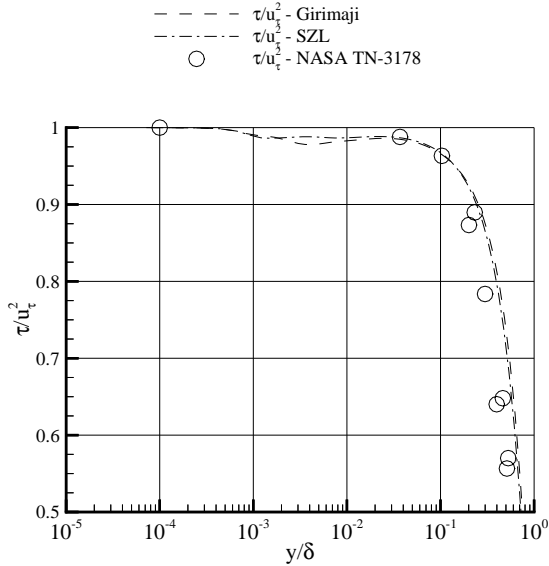


Figure 24. Detail of total shear stress in the boundary layer, $M = 0.4$, $R = 30$ million/ft.

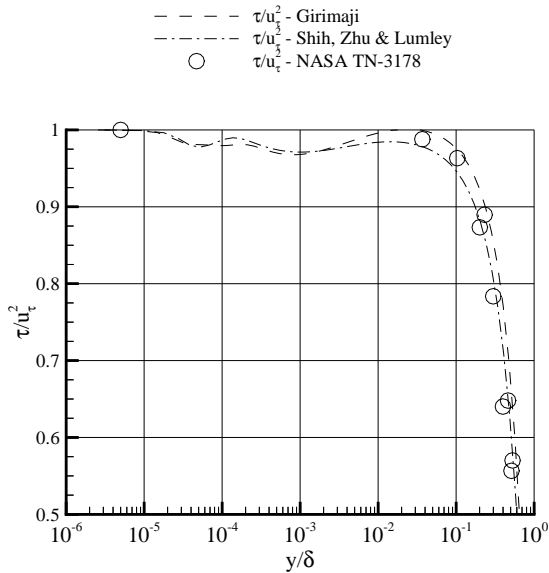


Figure 25. Detail of total shear stress in the boundary layer, $M = 1.2$, $R = 1$ million/ft.

Table 8. Wall values at $R_x = 444$ million, $M = 0.4$.

Model	u_w (m/sec)	τ_w (N/m ²)	u_t (m/sec)
Girimaji	1.426	220.6	4.173
SZL	1.189	183.8	3.812

Table 9. Wall values at $R_x = 14.2$ million, $M = 1.2$.

Model	u_w (m/sec)	τ_w (N/m ²)	u_t (m/sec)
Girimaji	4.303	21.91	14.217
SZL	3.864	19.65	13.491

CONCLUSION

Compressible Navier-Stokes solutions using two algebraic Reynolds stress turbulence simulations ranging from low to very high Reynolds numbers are transformed using several different semi-empirical methods to be compared with incompressible data. Calculations were performed on a 5-meter flat plate geometry at Mach numbers from 0.4 to 3.5 at unit Reynolds number from 1 to 30 million/ft. with zero pressure gradient free-stream flow. Solution convergence at each grid level was typically better than 0.00005 drag coefficient. Errors due to grid density were also typically within 0.00005 drag coefficient. Transition to turbulence was tracked and accounted for as an issue for overall drag. Both algebraic Reynolds stress models tested here provided consistent and well behaved solutions to very high Reynolds number throughout the Mach number range. The semi-empirical theories of van Driest and Sommer and Short both collapsed the computational compressible skin friction coefficients closely to a single line. While the turbulence model proposed by Girimaji has a slightly more physical basis than the theory by Shih, Zhu, and Lumley, the high Reynolds number skin friction coefficients predicted using Girimaji were typically high. At the lower Reynolds numbers 3 to 30 million, both turbulence models predicted skin-friction coefficients within 2% of the semi-empirical theories. At very high Reynolds numbers, 100 to 500 million, the turbulence model by Shih, Zhu and Lumley predicted skin-friction coefficients 6% less than the semi-empirical theories and Girimaji predicted coefficients 10% above the correlations.

REFERENCES

- Peterson, J.B., "A Comparison of Experimental and Theoretical Results for the Compressible Turbulent-Boundary-Layer Skin Friction with Zero Pressure Gradient," NASA TND-1795, March, 1963.
- Rubesin, M.W., Maydew, R.C. and Varga, S.A., "An Analytical and Experimental Investigation of the Skin Friction of the Turbulent Boundary Layer on a Flat Plate at Supersonic Speeds," NASA TN-2305, February, 1951.
- Wilson, R.E., "Turbulent Boundary-Layer Characteristics at Supersonic Speeds-Theory and Experiment," *Journal of the Aeronautical Sciences*, Vol. 17, No. 9,

- Sept. 1950, pp. 585–594.
- ⁴Chapman, D.R. and Kester, R.H., “Turbulent Boundary-Layer and Skin-Friction Measurements in Axial Flow Along Cylinders at Mach Numbers Between 0.5 and 3.6,” NACA TN-3097, March, 1954.
- ⁵Sommer, S.C., and Short, B.J., “Free-Flight Measurements of Turbulent Boundary-Layer Skin Friction in the Presence of Severe Aerodynamic Heating at Mach Numbers From 2.8 to 7.0,” NACA TN-3391, March, 1955.
- ⁶Abdol-Hamid, K.S., Carlson, J.R., and Lakshmanan, B., “Application of Navier-Stokes Code PAB3D to Attached and Separated Flows for Use with $K-\epsilon$ Turbulence Model,” NASA TP-3480, Jan. 1994.
- ⁷Abdol-Hamid, K.S., “A Multi-Block/Multizone Code (PAB3D-v2) for the Three-Dimensional Navier-Stokes Equations: Preliminary Applications,” NASA CR-182032, Oct. 1990.
- ⁸Abdol-Hamid, K.S., Carlson, J.R., and Pao, S.P., “Calculation of Turbulent Flows Using Mesh Sequencing and Conservative Patch Algorithm,” AIAA Paper 95-2336, July 1995.
- ⁹Carlson, J.R., “Application of Algebraic Reynolds Stress Turbulence Models Part I: Incompressible Flat Plate,” *Journal of Propulsion and Power*, Vol. 13, No. 5, 1997, pp. 610–619.
- ¹⁰Abdol-Hamid, K.S., “Implementation of Algebraic Stress Model in a General 3-D Navier-Stokes Method (PAB3D),” NASA CR-4702, Dec. 1995.
- ¹¹Launder, B.E., and Sharma, B.I., “Application of the Energy Dissipation Model of Turbulence to the Calculation of Flow near a Spinning Disk,” *Letters in Heat and Mass Transfer*, Vol. 1, 1974, pp.131–138.
- ¹²Girimaji, S.S., “Fully-Explicit and Self-Consistent Algebraic Reynolds Stress Model,” *Inst. for Computer Applications in Science and Engineering*, 95-82, Dec. 1995.
- ¹³Speziale, C.G., Sarkar, S., and Gatski, T.B., “Modeling the Pressure-Strain Correlation of Turbulence: An Invariant Dynamical Systems Approach,” *Journal of Fluid Mechanics*, Vol. 227, 1991, pp. 245–272.
- ¹⁴Shih, T-H., Zhu, J., and Lumley, J.L., “A New Reynolds Stress Algebraic Model,” NASA TM-166644, Inst. for Computational Mechanics, 94-8, 1994.
- ¹⁵Shih, T-H., and Lumley, J.L., “Remarks on Turbulent Constitutive Relations,” NASA TM-106116, May 1993.
- ¹⁶Gatski, T.B., and Speziale, C.G., “On Explicit Algebraic Reynolds Stress Models for Complex Flows,” NASA CR-189725, Inst. for Computer Applications in Science and Engineering, 92-58, Nov. 1992.
- ¹⁷Bradshaw, P., Editor, “Turbulence,” *Topics in Applied Physics*, Vol. 12, Springer-Verlag, New York, 1976.
- ¹⁸Schlichting, H., “Boundary-Layer Theory,” 7th ed., McGraw-Hill, New York, 1979, pp. 639–641.
- ¹⁹Rubesin, M.W., Maydew, R.C., and Varga, S.A., “An Analytical and Experimental Investigation of the Skin Friction of the Turbulent Boundary Layer on a Flat Plate at Supersonic Speeds,” NACA TN-2305, Feb. 1951.
- ²⁰Klebanoff, P.S., “Characteristics of Turbulence in a Boundary Layer with Zero Pressure Gradient,” NACA TN-3178, Jul. 1954.